NJC

Accepted Manuscript

This is an *Accepted Manuscript*, which has been through the Royal Society of Chemistry peer review process and has been accepted for publication.

Accepted Manuscripts are published online shortly after acceptance, before technical editing, formatting and proof reading. Using this free service, authors can make their results available to the community, in citable form, before we publish the edited article. We will replace this *Accepted Manuscript* with the edited and formatted *Advance Article* as soon as it is available.

You can find more information about *Accepted Manuscripts* in the Information for Authors.

Please note that technical editing may introduce minor changes to the text and/or graphics, which may alter content. The journal's standard Terms & Conditions and the Ethical guidelines still apply. In no event shall the Royal Society of Chemistry be held responsible for any errors or omissions in this *Accepted Manuscript* or any consequences arising from the use of any information it contains.

ROYAL SOCIETY OF CHEMISTRY

www.rsc.org/njc

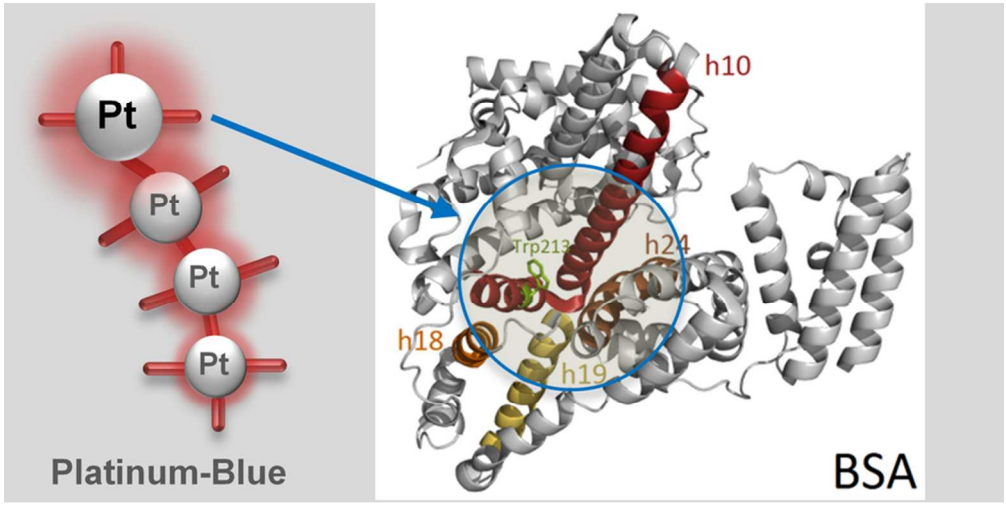

39x19mm (600 x 600 DPI)

Interaction of a Novel Platinum Drug with Bovine Serum Albumin: FTIR and UV-Vis Spectroscopy Analysis

Filiz KORKMAZ[a]✉, Deniz ALTUNOZ ERDOGAN[b1], Şeniz ÖZALP-YAMAN[b]

[a] Atilim University, Faculty of Engineering, Biophysics Laboratory, 06836, Ankara, Turkey

[b] Atilim University, Faculty of Engineering, Department of Chemical Engineering and Applied Chemistry, 06836, Ankara, Turkey

✉ **Corresponding Author**

E-mail: filiz.korkmaz@atilim.edu.tr

Phone: +90 312 5868552

[1] Present Address: Department of Chemistry, Bilkent University, 06800, Ankara, Turkey

ABSTRACT

Platinum complexes are proven to be very effective in cancer treatment. However, severe side effects of these drugs lead scientists in pursuit of new platinum complex derivatives. A novel blue platinum compound, called Platinum-Blue (Pt-Blue), is one of the promising candidate platinum compounds to be used for tumor treatment. In this study the interaction of Pt-Blue with bovine serum albumin (BSA) has been investigated using UV-Vis and FTIR spectroscopy. One of the findings is that the drug-protein interaction type depends on the drug concentration. While Pt-Blue is attached to the surface of BSA at high concentrations; it interacts with a hydrophobic region of the protein at low concentrations with a binding constant of $1.93x10^5$ M^{-1}. Spectroscopic results indicate the hydrophobic docking position to be around Trp 213 in domain II, which is surrounded by a number of Asp and Glu. During this interaction, helices like helix-10, helix-18, helix-19 and helix-24 change orientation and/or partially unfold to make room for the compound. Binding constants at high and low concentrations of Pt-Blue are determined using UV-Vis spectroscopy, which are found to be comparable to cisplatin. FTIR spectroscopy also reveals that the interaction between Pt-Blue and BSA is noncovalent, which makes the candidate drug favorable since it is available for DNA binding while being carried by albumin.

Keywords: Serum albumin, Platinum-Blue, anticancer drug, FTIR spectroscopy, drug-protein interaction

1.INTRODUCTION

Among the anti-cancer agents, platinum-based drugs are the most effective in the treatment of various malignancies and cancer patients [1]. Currently there are three main cisplatin derivatives approved by FDA. Carboplatin [2] and nedaplatin [3] are more easily administrated and less toxic than cisplatin [4,5]. Oxaliplatin, on the other hand, has a different spectrum of activity compared with cisplatin [6] and has been used for the treatment of metastatic colorectal cancers in European countries [7]. Although patients initially respond well to these agents, these drugs cause toxicity and many patients develop drug resistance shortly after the treatment [8]. Because of such clinical inconveniences associated with cisplatin, some of cisplatinum derivatives have entered the clinic in search for an agent that is effective enough but has less toxicity. A family of deeply colored platinum compounds, usually called platinum blues, has attracted the interest of researchers because of their unusual color and high antitumor activities [9]. In contrast to the usual yellow, orange, red, or colorless platinum complexes, platinum blues are unusual for their intense blue or purple colors [10]. The first blue platinum compound was synthesized by German chemists in 1908 [11]. This unusual material was first proposed to have a mononuclear composition of $Pt^{II}(CH_3CONH)_2.H_2O$. However, the compound was later proposed to be polymeric with bridging acetamidate linkages [12]. Moreover, special attention was paid to the platinum blues produced from the reactions between the hydrolysis product of cis-DDP (i.e., cis-$[Pt(NH_3)_2(OH_2)_2]^{2+}$) and pyrimidine bases such as uracil, since these so-called "platinum-pyrimidine-blues" were found to have a high index of antitumor activity with a lower associated nephrotoxicity than cis-DDP [1].

The interaction of DNA with the novel Pt-Blue complex, $[Pt_2(2atp)_4(H_2O)(OH)]$ (Fig. 1) has been studied previously by spectroscopic and electrochemical techniques. Decrease in molar absorptivity (hypochromism) by about 31% with a slight red shift is ascribed as the strong binding of the blue complex by intercalation of aromatic ligand between base pairs of nucleic acid [13–15]. The cleavage behavior of the blue complex on plasmid DNA is monitored by agarose gel electrophoresis. The preliminary results indicate that Pt-Blue complex is able to perform direct double-strand cut in the

presence of a reducing agent, mercaptopropionic acid (MPA), in 25 nM concentration. Moreover, the Pt-Blue complex inhibits the GST enzyme activity between 600-700 nM [16]. Besides their function of detoxification, GST enzymes are also responsible for drug resistance and therefore, inhibition of this enzyme with Pt-Blue complex suggests that it can be used in combined chemotherapy as well. However, detailed studies are still being continued on the subject to determine the binding mechanism of the complex on DNA.

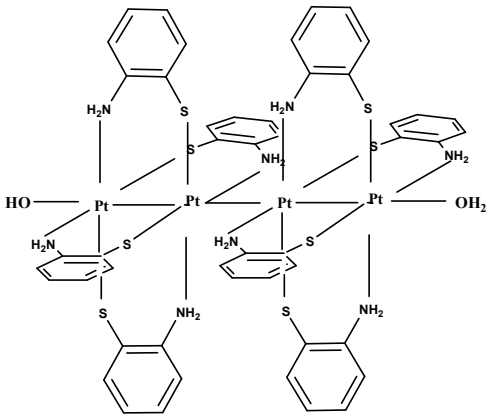

Figure 1: Molecular structure of Platinum-Blue (Pt-Blue).

Investigation of such candidate anti-cancer drugs in terms of their binding properties on blood proteins is important, since all such agents are applied intravenously in cancer treatment and they are carried by plasma proteins [17]. Pt-Blue is a cationic molecule, thus an anionic protein like serum albumin is seen as a likely candidate to interact with the drug. Serum albumins are the most abundant proteins in mammals and therefore, are the most studied protein in literature. Owing to the remarkable capacity of binding, serum albumins are responsible for the transportation and distribution of various ligands, drugs, nutrients and other molecules [18]. In this study, bovine serum albumin (BSA) is used to investigate the binding properties of Pt-Blue and the effect of this interaction on the structure of the protein is reported. Although bovine and human serum albumins are only analogous to some extent, the difference is hardly on the surface. Thus the affinity and binding properties do not differ much between them [19].

BSA is mainly a helical protein with 74 % α-helix and 26 % unordered structure and turns with no contribution of β-sheet type of folding (PDB Id: 3V03) [19]. BSA has several aspartic and glutamic acid residues exposed on the surface. They are responsible from carrying 45% of circulating Ca^{2+} (2.4 mM) and Mg^{2+} (1.2 mM) [20]. The binding sites are in domain I and are coordinated by side chains of aspartic and glutamic acids [19].

In this study, we have investigated the binding properties of Pt-Blue, containing 2-aminothiophenol, to BSA with electronic absorption spectroscopy. The binding constant at different concentrations of the drug is tested under physiological conditions. The effect of binding on the structure of BSA is studied with Fourier Transform Infrared (FTIR) spectroscopy. FTIR spectroscopy is widely used to study the structure and dynamics of proteins, lipids, enzymes and their interaction with ligands [21–24]. Pt-Blue is incubated with BSA for 15 days to inspect time-dependent changes (if any) on BSA structure.

2.MATERIALS AND METHODS

2.1Platinum-Blue (Pt-Blue) Synthesis. To the best of our knowledge, the reaction of tetrachloroplatinate(II), $[PtCl_4]^{2-}$, with 2-aminothiophenol (atp) has been investigated for the first time by our group [16]. Elemental analysis, UV-Vis, IR, ESR, ESCA, SEM, ^{1}H-NMR, ^{13}C-NMR, ^{195}Pt-NMR and electrochemical analysis performed on this dark blue colored compound (Fig. 1) suggest that it is a new "platinum blue" type complex, $[Pt_2(2atp)_4(H_2O)(OH)]$ [16]. The intense characteristic peak in the visible region at 724 nm, which is responsible for its blue color in electronic absorption spectrum, is assigned to an allowed metal-metal charge transfer due to the Pt^{II}-Pt^{III} mixed valance character of the complex [25]. Solid state ESR spectrum shows the complex to be paramagnetic, indicating a mixed-valence character, one unpaired electron is coming from a Pt(III) atom. Details of the synthesis and analysis can be found elsewhere [16].

2.2 Electronic Absorption Measurements. Electronic absorption spectra of the Pt-Blue are recorded in the absence and presence of BSA in 0.1M sodium phosphate (NaPi) buffer at pH 7.4 by

using Agilent 8453 UV-Vis spectrophotometer. For titration experiments, samples are prepared by first selecting a specific drug concentration. After that, increasing amount of BSA solution is added while keeping the total volume of the solution constant (10 mL). For control experiments, the reverse sets of experiments are also performed. Samples of constant volume (10 mL) are prepared by increasing the drug concentration, while keeping the BSA concentration constant. In the experiments, the ratio of the BSA to the drug concentration (R = [BSA] / [DRUG]) is varied from 0.2 to 10. The electronic absorption spectra are recorded for each R value after 30 minutes of incubation. Due to Pt-Blue absorption at around 280 nm at high concentrations of the drug corresponding to the range of R values from 1 to 0.2 (Fig.S-1b), spectra are corrected by subtracting Pt-Blue absorbance from that of the BSA+Pt-Blue adduct prior to the binding constant calculation. However, such a correction is not necessary for samples having low drug concentrations, i.e., for the range R = 1 through R = 6.5.

2.3 FTIR Spectroscopy Measurements. BSA is dissolved in 0.1 M NaPi buffer, pH 7.4 to get a final concentration of 0.15 mM. Appropriate amount of powder Pt-Blue is weighed and added on BSA solution so that the final molar ratio of protein to compound is six (R = 6). BSA blank and BSA+Pt-Blue samples are incubated for 15 days using a heated, circulating water bath at 37 °C. The next day, another set of the same samples is prepared identically as the first set and incubation starts. Similarly, a third set of samples is prepared on the third day. This way, there are three sets of samples (blank BSA and BSA+drug) all incubated at physiological conditions, so that every experiment is performed three times. Samples are measured hourly in the first six hours of incubation and afterwards measured daily at the same hour of the day during the 15 days incubation period.

5 µl of the sample is dried on CaF_2 cells under constant mild N_2 blow for 15 min. This process is used to vaporize the excess water in samples and provided better visualization of amide-I and –II profiles of the sample. A second CaF_2 cell is used to sandwich the sample and the infrared (IR) absorbance spectrum is recorded with Nicolet 6700 (Thermo Fisher Scientific Inc., USA)

spectrometer equipped with a DTGS detector. 256 scans are averaged for a final resolution of 2 cm^{-1}. The sample chamber inside the spectrometer is constantly purged with dry air. An empty pair of CaF_2 cells is used for background measurement, which is subtracted automatically by the software OMNIC 8.2 (Thermo Fisher Scientific Inc.).

2.4FTIR Spectra Processing

Difference. The water absorption is corrected when necessary by subtracting the appropriate buffer spectrum. In difference spectra calculation, absorbance due to CH_2 symmetric and antisymmetric modes in the range 2950-2800 cm^{-1} is taken as the reference so that a flat line in this region indicated a successful subtraction. This region is chosen because the interaction between BSA and Pt-Blue should not affect the number and property of CH_2 modes originating from side chains, thus the absorbance in this region.

Side Chain Subtraction and Curve Fitting. Subtraction of side chain contributions from the IR spectrum of the protein has been performed according to the method documented previously [21,26]. Side chains such as Asp, Glu, Tyr, His, Phe, Gln, Asn, Arg and Lys give rise to bands in amide-I and -II regions and their position change when the buffer is switched from H_2O to ^2H_2O-buffer. Since the spectra of BSA equilibrated in ^2H_2O-buffer are used for secondary structure analysis, contributions of these side chains are subtracted. However, the side chains residing in hydrophilic region (protein surface) are deuterated but those in hydrophobic region are not affected by ^2H_2O-buffer and thus, they give rise to IR bands at different positions. Therefore, the number of above listed amino acids in hydrophilic and in hydrophobic regions are first determined from the crystal structure of BSA (PDB ID: 3V03) and their spectral contributions are generated according to the parameters reported earlier [27] and subtracted from the BSA spectrum.

Although Pt-Blue has characteristic signals in the fingerprint region of the infrared spectrum (Fig. 6iii), these contributions can not be subtracted from the spectrum of BSA+Pt-Blue complex. The signal at 1655 cm^{-1}, attributed to C=C stretching mode in Pt-Blue, is attempted to subtract. For this

subtraction, another Pt-Blue signal at 1392 cm^{-1} is taken as reference. Complete or even partial disappearance of this band yields a bizarre amide-I profile. When the Pt-Blue sample is dried exactly like any BSA sample, the signal at 1655 cm^{-1} disappears completely from the spectrum. This can be explained by the ring orientation with respect to the electric field propagation direction. Since excess water in all BSA samples is removed prior to every experiment, we assume that Pt-Blue contribution does not interfere with amide-I profile of the protein.

For the curve-fitting analysis, the number of sub-bands under the amide-I and-II complex bands is determined from the second derivative of spectra to be fitted. Fitting is performed with the software OMNIC 8.2. A mixture of Gaussian and Lorentzian band shape is chosen for each sub-band. Intensity and position of sub-bands are pre-determined; however, the width and shape of bands are determined by the software so that the best fit is obtained. Fit success is determined by comparing the raw spectrum and the composite spectrum, which is the spectral sum of all fitted sub-bands.

3.RESULTS AND DISCUSSION

3.1 BSA—Pt-Blue interaction differs at high and low concentrations. The application of electronic absorption spectroscopy is one of the useful methods for defining protein–binding properties. The acting forces between a small molecule and protein are mainly H-bond, van der Waals force, electrostatic and hydrophobic forces [28]. In order to discover the mode of action and the structural change of BSA upon addition of the complex, the electronic absorption spectra of BSA are measured with different amounts of Pt-Blue complex. The spectral change on the absorption spectrum of BSA upon the addition of the Pt-Blue complex is depicted in Figures 2 and 3.

Two types of interaction between BSA and Pt-Blue are predicted depending on the concentration of Pt-Blue. The electronic absorption spectrum of BSA consists of an intense absorption band at around 280 nm, due to the aromatic tryptophan and tyrosine [29] residues (Fig S-1). The most efficient incubation time and the molar ratio of the protein to the complex (R = [BSA]/[Pt-Blue]) are determined by spectroscopic titration by keeping the BSA concentration constant in the presence of

Pt-Blue in various concentrations and inversely, by fixing the concentration of Pt-Blue with varying BSA concentrations. Both experimental results indicate the threshold limit of the drug as R = 6 - 6.5 with 30 min of incubation time at 37 ^{o}C. Hence, spectroscopic titration experiments (Fig. 2) that are carried out for R = 1 to R = 6.5 reveal that the intensity of the characteristic band of BSA at around 280 nm decreases upon the addition of lesser amount of Pt-Blue, from 2.13x10^{-5} (R = 1) to 3.27x10^{-6} M (R = 6.5) in NaPi buffer pH 7.4.

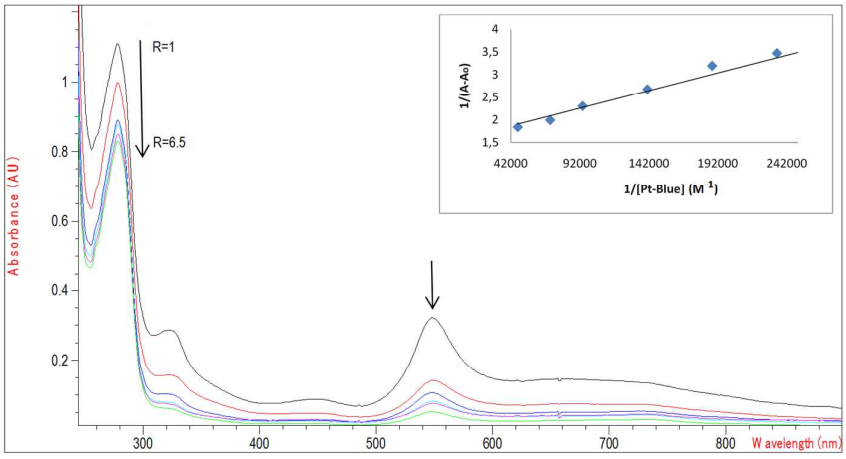

Figure 2. The change in the electronic absorption spectrum of BSA upon the addition of Pt-Blue for values of R = 1, 2, 3, 4, 5 and 6.5 in NaPi buffer (pH 7.4) at 37 °C incubated for 30 min. Inset shows the plot of 1/(A-A_0) *vs.* 1/[Pt-Blue] at 280 nm for the calculation of binding constant of the Pt-Blue complex to BSA for the same R values.

The observed hypochromism (decrease in absorption intensity; A=1,1069 to 0.83023 a.u.) with a slight shift in the wavelength indicates binding of the Pt-Blue to hydrophobic sites of the protein and thereby altering the conformation of BSA [30,31]. It may also designate that the polarity around the tryptophan residue is increased and the hydrophobicity is decreased [32].

The binding constant of Pt-Blue to the protein, K_b, can be determined from the spectral changes;

$$\text{BSA} + \text{Pt-Blue} \rightarrow \text{BSA:Pt-Blue}$$

$$K_b = \frac{[BSA{:}\text{Pt}-\text{Blue}]}{[\text{BSA}]\,[\text{Pt}-\text{Blue}]}$$

The plot of $1/(A-A_0)$ versus 1/[Pt-Blue] is linear and the binding constant K_b can be estimated from the ratio of the intercept to the slope (Fig 2, inset), where A_0 is the initial absorption of the blank BSA at 280 nm in NaPi buffer pH 7.4 and A is the absorption values measured at different Pt-Blue concentrations ([Pt-Blue]). The overall binding constant for BSA:Pt-Blue adduct is calculated to be $1.93x10^5$ M^{-1}. The binding constant estimated for BSA:Pt-Blue adduct shows strong complex protein interaction as observed for other drug-BSA adducts with binding constants ranging from 10^5 to 10^6 M^{-1} [22,28,33–36].

On the other hand, the intensity of the characteristic band of BSA increased upon addition of increased amount of Pt-Blue, between $2.13x10^{-5}$ and $1.07x10^{-4}$ M, which corresponds to *R* values between 1 and 0.2, respectively (Fig. 3). This hyperchromic effect (increase in absorption intensity; A=1.1069 to 2.6143 a.u.) reveals that the platinum complex is attached on the protein surface by external contact, most probably via electrostatic interaction to the secondary structure of the protein [22,37]. The observed hyperchromic effect may also be suggestive of an increase in exposure of tryptophan to the solvent [38]. Prior to the determination of the binding constant of Pt-Blue as $1.20x10^5$ M^{-1} (Fig. 3-inset), the absorption data is corrected since Pt-Blue complex has high absorption at low *R* values in the same region (Fig. S-1b).

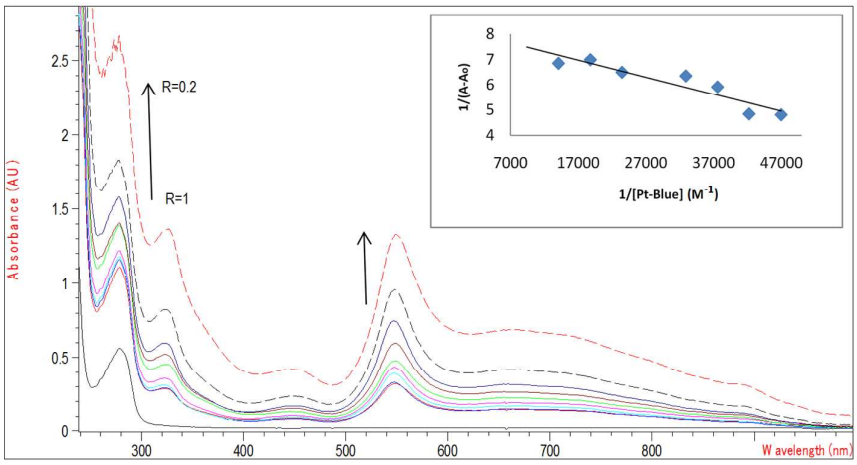

Figure 3. The change in the electronic absorption spectrum of BSA upon the addition of Pt-Blue (*R* = 1, 0.9, 0.8, 0.7, 0.6, 0.5, 0.4, 0.3 and 0.2) in NaPi buffer (pH 7.4) at 37 °C incubated for 30 min.

Inset shows the plot of $1/(A-A_0)$ *vs.* 1/[Pt-Blue] at 280 nm for the calculation of binding constant of the Pt-Blue complex to BSA (R = 1 to 0.2).

3.2 BSA─Pt-Blue interaction at low concentrations

Structural properties of BSA: FTIR spectroscopy is used to determine the secondary structure changes in BSA upon Pt-Blue addition. BSA with and without Pt-Blue incubated for 15 days are also monitored by FTIR spectroscopy. Proteins give rise to many signals in the mid-IR region; however, the most frequently used bands for the secondary structure analysis are the amide-I (1700-1600 cm^{-1}) and amide-II (1600-1500 cm^{-1}) bands. Amide-I band arises due to C=O stretching modes, originating from polypeptide backbone of proteins, thus gives information about the secondary structure. Amide-II band is a mixture of C-N stretching coupled with N-H bending modes, again due to protein backbone. Amide-II band is generally used for $^{1}H/^{2}H$ exchange rate determination of a given protein.

IR absorbance spectrum of BSA together with its second derivative profile is shown in Figure 4. Amide-I band is the sum of smaller bands originating from different secondary structure elements and side chain contributions of some residues; so it is a complex band by nature. Calculating second derivative is one of the mathematical approaches to resolve the underlying bands. Any individual signal under the amide-I is reflected as a negative peak in the second derivative profile.

While the amide-I band of BSA is overwhelmed by the band located at 1657 cm^{-1}, amide-II band is mainly characterized by the band at 1542 cm^{-1}, both indicating a predominantly α-helical structure, in accordance with previous studies [19,39]. Other signals observed in the second derivative of amide-I and –II bands originate from turns, loops and side chain modes of certain residues. The second derivative profile is used to resolve the underlying peaks under complex bands but determining the percentage fraction of each sub-band requires curve fitting of amide-I.

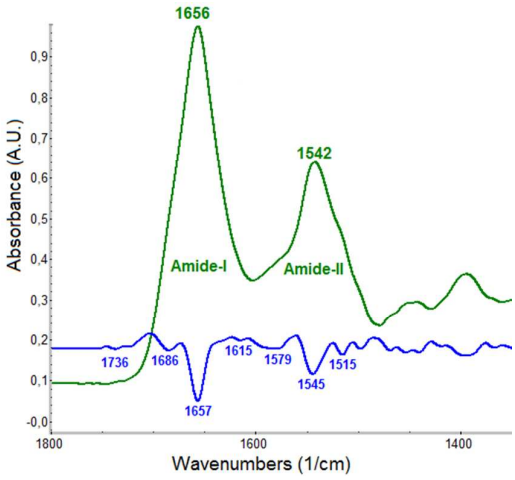

Figure 4: Fingerprint region of infrared absorbance spectrum of BSA (green) in NaPi pH 7.4 buffer at 37°C and its second derivative profile (blue). The second derivative profile is magnified in vertical axis for better comparison with the absorbance spectrum.

BSA—Pt-Blue Complex: In order to study the effect of Pt-Blue on BSA structure and time dependence of these changes, we have first investigated the structural stability of BSA during an incubation period of 15 days. The amide-I and amide-II profiles of BSA blank do not show any time dependent changes at physiological conditions during the time of incubation (Figure 5a). However, these positions slightly change by the addition of Pt-Blue; shifting amide-I and amide-II to 1658 cm^{-1} and 1540 cm^{-1}, respectively (Figure 5b). While the secondary structure of BSA is certainly affected by the presence of Pt-Blue, as indicated by peak position shifts, these are instant changes and the position of amide bands do not further shift during the incubation period. However, there are additional changes in the overall shape of amide-I band and at the border between amide-I and amide-II, starting at the 6^{th} day of incubation.

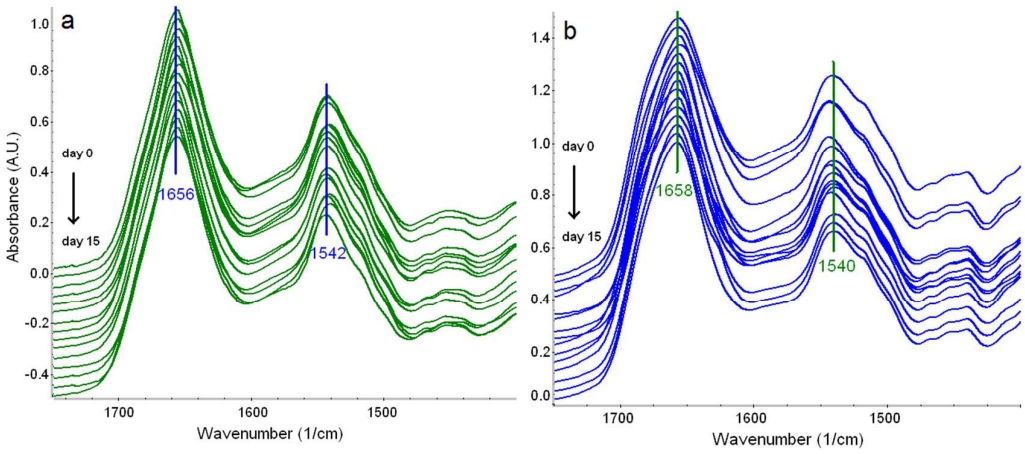

Figure 5: Collection of spectra during the incubation time, showing amide-I and –II profile of BSA blank (a) and BSA in complex with Pt-Blue (b). Samples are in NaPi buffer pH 7.4 at 37 °C. Spectra are evenly spaced along the vertical axis for better visualization of the time-dependent progress of spectra.

In order to understand the time dependent structural changes in BSA induced by Pt-Blue in the course of incubation, we first start with the instant changes induced by the Pt-Blue addition at the beginning of incubation (2nd hour). Figure 6 shows the absorbance spectrum of BSA with and without Pt-Blue in H_2O buffer. Addition of Pt-Blue up-shifted the position of amide-I band by 2 cm^{-1}. When the difference spectrum in the same buffer (Fig. 6v) is calculated, a negative feature around 1653 cm^{-1} and positive features at 1675 and 1685 cm^{-1} are seen to be the reason of the amide-I position shift. These changes are argued to represent the conversion of some of the ordered secondary structure to unordered structure. In order to validate this assumption, a similar difference spectrum is also calculated in ^2H_2O buffer. The positive feature at 1643 cm^{-1} confirms the existence of more unordered structure upon the addition of Pt-Blue. On the other hand, C=O stretching mode of Asn/Gln is also consistent with these spectral changes. The negative bands at 1663, 1653, 1542 and 1547 cm^{-1} in two buffer conditions suggest that some of the long helices, at least partially unfold and become unordered.

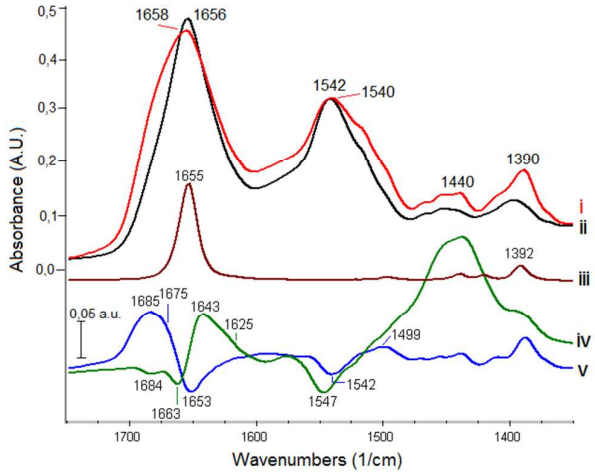

Figure 6: Absorbance spectra of BSA with (i) or without Pt-Blue (ii) in NaPi-H_2O buffer, pH 7.4. Absorbance of Pt-Blue in NaPi-^2H_2O buffer pH 7.4 is shown as the middle trace in the figure (iii) in order to pinpoint the signals originating from Pt-Blue structure in difference spectra. The difference of absorbance spectra in ^2H_2O buffer (iv) and in ^1H_2O buffer (v) is calculated to show only the changes in BSA structure. Positive features in difference spectra are introduced by the Pt-Blue addition.

Pt-Blue has also signature absorptions at 1655 (strong), 1498 (weak), 1440 (weak), 1421 (weak) and at 1392 cm^{-1} (medium) (Fig. 6iii). The strongest one at 1655 cm^{-1} is suggested to originate from C=C stretching mode. The signal at 1498 cm^{-1} is attributed to C-ring of the molecule. The presence of Pt-Blue in the difference spectra (Fig. 6iv & 6v) is clearly seen by the signals at 1498 and 1392 cm^{-1}. However, the signal at 1655 cm^{-1} due to C=C stretching mode of Pt-Blue is missing in the same spectra. When the blank Pt-Blue sample is dried, the same signal also disappears from the spectrum as well, probably due to its dipole moment orientation with respect to the electric field propagation direction.

In order to understand the structural changes at later stages of the incubation, BSA spectrum is compared with selected BSA in complex with Pt-Blue sample spectra (Fig. 7). As pointed out in the analyses shown above, the structure of BSA shows instant changes upon Pt-Blue addition; however, starting at the 6^{th} day of incubation, there are further changes. For this reason, four spectra are selected form the incubation series; the spectrum at the 5^{th} day, 6^{th} day, 9^{th} day and at the 15^{th} day.

While the spectra of BSA are exactly the same over the time of incubation, amide-I profiles of BSA with Pt-Blue samples are larger due to a clear hump at ~1685 cm^{-1}. The second derivative profiles of these spectra are shown in Figure 7b. The hump is clearly seen to be the 1685 cm^{-1} band that grows dramatically after the 6th day of incubation. Another change starting at the same time is the slight growth at position 1600 cm^{-1}. The shape of the upper border of amide-II (1570-1600 cm^{-1}) is the same among BSA samples and BSA with Pt-Blue at the beginning of incubation until the 6th day. Spectra taken after the 6th day have bigger amplitude around 1600 cm^{-1}. Furthermore, the lower frequency region of amide-I (1600-1640 cm^{-1}) is also observed to get less populated compared to early stages of incubation. The second derivative profile (Fig. 7b) also shows changes around 1592 cm^{-1} and enlargement at the lower frequency skirt of 1656 cm^{-1}, approximately around 1640 cm^{-1}.

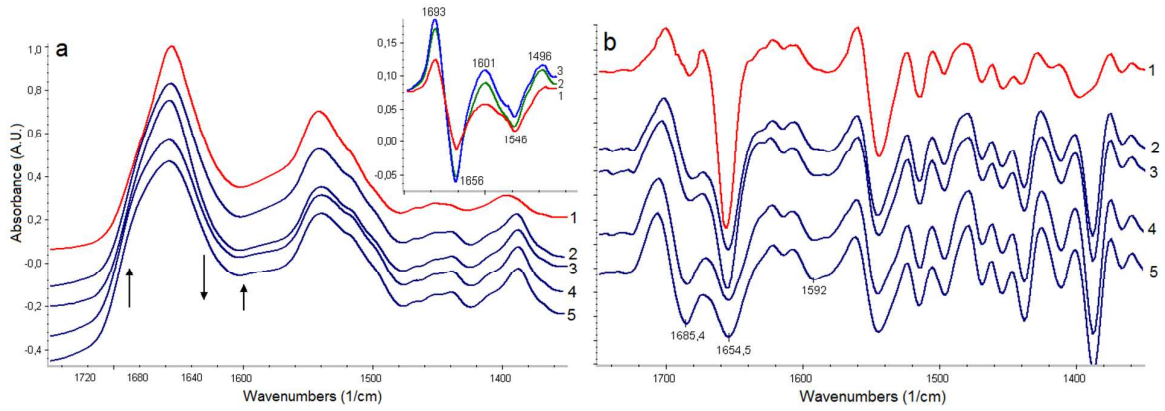

Figure 7: Absorbance spectra of BSA at 6th hour (1) of incubation together with spectra of BSA in complex with Pt-Blue at 5th day (2), 6th day (3), 9th day (4) and 15th day (5) of incubation (a) in NaPi-H_2O buffer, pH 7.4. The corresponding second derivative profiles of the same spectra are also shown in the same order (b). Spectra are offset corrected for better comparison along the vertical axis. The inset figure shows difference spectra of BSA with Pt-Blue at 6th day *minus* the 5th day (red/1), 9th day *minus* the 5th day (green/2) and 15th day *minus* the 5th day (blue/3).

To be able to distinguish spectral differences starting at the 6th day of incubation, difference spectra relative to 5th day are calculated. Figure 7a-inset shows spectral differences of the 6th day,

9^{th} day and 15^{th} day relative to the 5^{th} day of incubation. All spectra show positive and negative features at close frequency positions but with enhanced amplitudes in time. The amplitude is almost constant between the 9^{th} day and the 15^{th} day, thus observed changes start at the 6^{th} day of incubation and are almost completed at the 9^{th} day. The common negative feature at 1656 cm^{-1} together with positive features around 1640 cm^{-1} (Fig. S-3) are argued to be originating from hydrophobic helices that are exposed to solution upon Pt-Blue interaction. Another positive signal at 1693 cm^{-1} can be interpreted as the intermolecular β-sheet, showing increasing contacts among ordered structure elements or it can as well be due to side chain modes of Gln, Asn and in some cases Arg [40]. Judging by the amplitude of this band, we suggest that it is a superposed band showing the changes around loops/turns together with side chain modes.

Secondary Structure of BSA Blank and in Complex with Pt-Blue: The secondary structure of BSA has been previously reported to be 74% helical with no β-sheet [19]. Out of 433 residues in helical form, most are part of long helices (14 to 42 amino acids (a.a.)-long) but some are part of short helices (5 to 10 a.a.-long), and some are in the form of 3_{10} helices. Approximately 50 residues take part in turns and the rest (~100 a.a.) are unassigned to a secondary structure, which are presumably in the form of unordered structure. In terms of percentage fractions, BSA is composed of 58% long helices, 12% short helices, 5% 3_{10} helix, 17% unordered structure and 8% turns based on X-ray data. In FTIR spectroscopy, helices having different lengths (long/short) and different environment (hydrophilic/hydrophobic) give rise to different signals in amide-I region [41–45]. Thus, these percentage fractions are used in assigning the fitted sub-bands to certain secondary structure elements.

The curve fitting of amide-I band of BSA has been performed after the spectrum is buffer corrected and side chain contributions are subtracted. Trying to reconstruct the underlying bands under the complex superposed amide-I band is certainly a challenge; however, assigning these bands to certain vibrational modes is another. Considering this difficulty, samples are analyzed in $^{2}H_2O$-buffer in order to discriminate different secondary structure elements and band assignments

are done by taking X-ray data as reference. The results of curve fitting are presented in Table 1. The area of each underlying band is given in terms of its percentage share within the total amide-I band area. Figure S-2 in supporting information section also shows the overall amide-I band, fitted sub-bands and the spectral sum of sub-bands to compare with the raw spectrum.

Table 1: Curve fitting results of BSA blank and BSA with Pt-Blue incubated for 15 days in $^{2}H_2O$ buffer. The percentage fraction of each fitted band is calculated by rationing the area of the sub-band to that of the total amide-I area. Secondary structure assignments are based on the X-ray data of BSA and previous FTIR studies [22,34,46].

IR signal position	Assigned secondary structure	BSA (%)	BSA & Pt-Blue (%)	BSA, X-Ray Data (%)
~1630 cm^{-1}	3_{10} helix; short helix;	15	16	4.5+12+17[†]
1640/1636 cm^{-1}	Solvent exposed short helix; unordered	2	17	
1652/1655 cm^{-1}	α-helix	75	57	58
~1675 cm^{-1}	Hydrophobic loops; turns	8	10	8

[†] BSA is composed of 3_{10} helices (4.5%), short helices of 5-10 a.a.-long (12%) and unordered structure (17%). IR signals of these structures are all located in the same region of the spectrum; 1630-1645 cm^{-1} under the amide-I band and therefore, an exact peak position for each cannot be given.

Amide-I components of BSA spectrum reveal that BSA is ~75% α-helical as indicated by the component at 1652 cm^{-1}. There is also a small contribution to the amide-I from 1640 cm^{-1} by 2 %, which is assigned to solvent exposed short helices [41,47] and unordered structure [21]. The component located at 1630 cm^{-1} is assigned to short helices and 3_{10} helix [48] that has 15% share in the total amide-I band. This band is also representative of intermolecular β-sheet, which is due to the contacts among helices [41]. Turns are reflected by signals located in 1670-1685 cm^{-1} range [24], therefore the band at 1675 cm^{-1} represents turns. 8% of the secondary structure is then assigned to turns. The fraction of turns, as revealed by FTIR spectroscopy, is equal to the fraction given by the X-ray crystallography results. On the other hand, the unordered structure cannot be distinguished

from the α-helix although the resolution of the spectrum and error of fitting are both low enough. Their combination gives one single peak at 1652 cm^{-1}, which is between the hypothetical positions of α-helix (~1657 cm^{-1}) and unordered structure (~1640 cm^{-1}) [49]; yet it is closer to helix position, indicating higher helical content. Therefore the fraction of helices and unordered structure cannot be compared with the X-ray data for BSA blank.

Introduction of Pt-Blue affects the secondary structure distribution as shown in Table 1. Curve-fitting analysis revealed that α-helix and unordered structure can now be distinguished. The signal at 1655 cm^{-1} is assigned to long helices, which comprises 57% of the structure; and unordered structure is assigned to the band at 1636 cm^{-1} based on the comparison of fractions with X-ray data, which has 17% fraction in the total amide-I band. These numbers are almost in perfect agreement with X-ray data of BSA, which proves that Pt-Blue interaction does not cause major changes in the structure of BSA. We suggest that Pt-Blue causes some helices to be solvent exposed so that the corresponding peak can be better distinguished. Not only the fractions but also the peak positions of the two peaks change. 1652 cm^{-1} shifts to 1655 cm^{-1}, and 1640 cm^{-1} shifts to 1636 cm^{-1}. These shifts in opposite directions clearly indicate that a peak approximately located around 1650 cm^{-1} shifts to around 1635 cm^{-1} judging by the percentage fraction of changes, which would mean increased hydrophilicity around some short helices with/without partial unfolding. Unfortunately it is not possible to quantify the number of amino acids involved in unfolding, if there are any; however, it cannot be a major unfolding of helices since the thermal stability of protein does not change upon interacting with Pt-Blue (unpublished data). The fraction of turns and short helices seem to be increased by 2% and 1%, respectively, compared with the curve-fitting results of BSA. Curve-fitting analysis suggests that changes introduced by Pt-Blue are the re-arrangements of ordered structures rather than conversion of one structure to another.

4.CONCLUSIONS

In this study, initially the effect of Pt-Blue on BSA has been investigated at different molar ratios by UV-Vis spectroscopy. We have found that the interaction mechanism between BSA and Pt-Blue is different for $R < 1$ and $R > 1$. For values of R between 1.0 and 6.5, Pt-Blue is found to interact with hydrophobic sites of the protein and hence changes the conformation of BSA. On the other hand, Pt-Blue is attached to the surface of protein via electrostatic forces for R values between 1.0 and 0.2. The binding constants at both R ranges are in the order of 10^5 M^{-1}, comparable to the binding constant of cisplatin.

We have also investigated the changes in BSA structure with FTIR spectroscopy at $R = 6$, at which the maximum binding occurs with Pt-Blue. The changes in the structure of BSA can be classified as 'instant' and 'late' effects. Instant changes are shown by the amide-I and amide-II band analysis of samples in H_2O and ^2H_2O buffer (Fig. 6). The positive feature at 1685 cm^{-1} in H_2O and at 1643 cm^{-1} in ^2H_2O buffer is either due to C=O stretching mode of Asn/Gln, or increased unordered structure due to partial unfolding of some helices, or the combination of both. A decrease in the fraction of long and/or hydrophobic helices has also been found in the same analysis. The slight shift of both amide-I and –II bands also supports the above findings (Fig. 5).

On the other hand, starting at the 6^{th} day of incubation, there are additional (late) changes regulating the interaction of Pt-Blue with BSA (Fig. 7). Additional decrease in the fraction of hydrophobic long helices is revealed by the difference of spectra from four chosen days of incubation. There are also changes in contacts among helices (intermolecular β-sheet). Intermolecular β-sheet is evident from the difference spectra by a pair of signals located at 1630 (overlapped under 1601 cm^{-1}, Fig. S-3) and 1693 cm^{-1}, which is suggested to be the result of helical re-arrangements to make way for the Pt-Blue docking. Results of UV-Vis spectroscopy also suggested that Pt-Blue interacts with hydrophobic sections of the protein, which is so far consistent with the results of FTIR study. In this study we could not detect any protonation/deprotonation changes around Asp and Glu, which are good candidates in coordinating and binding to cationic

molecules. Although there are IR absorbance changes in the range 1570-1600 cm^{-1}, there are no changes in the range 1700-1740 cm^{-1} that should accompany upon H-bonding. Therefore, deprotonated Asp and Glu are suggested to coordinate Pt-Blue only by noncovalent interactions.

In an earlier study with a positively charged Platinum complex interacting with human serum albumin, the drug was shown to interact with Trp214, located in a hydrophobic cavity in domain IIA [50]. When the primary structure of BSA is analyzed, there are only two Trp residues ~~(Fig. 8a)~~; the first (Trp134) is located on the surface ~~(Fig. 8b)~~, facing the hydrophilic interface, and the second Trp residue (Trp213) is located in a hydrophobic pocket (Fig. 8a) surrounded by negatively charged residues (Fig. 8~~C~~b). UV-Vis spectroscopy data and FTIR results in this study suggest that Pt-Blue interacts with a hydrophobic cavity in BSA. Since Pt-Blue is a cationic molecule, it is only natural to assume that the cavity should be rich in negatively charged residues. In this respect, the cavity including Trp 213 and surrounded by helices h10, h18, h19 and h24 is a possible docking position for Pt-Blue. Thus we propose that Pt-Blue is coordinated by negatively charged residues located in this pocket (Fig. 8~~c~~b), so that some initially hydrophobic helices like h10, h18, h19 and h24 are exposed to solution to make way for the drug during docking.

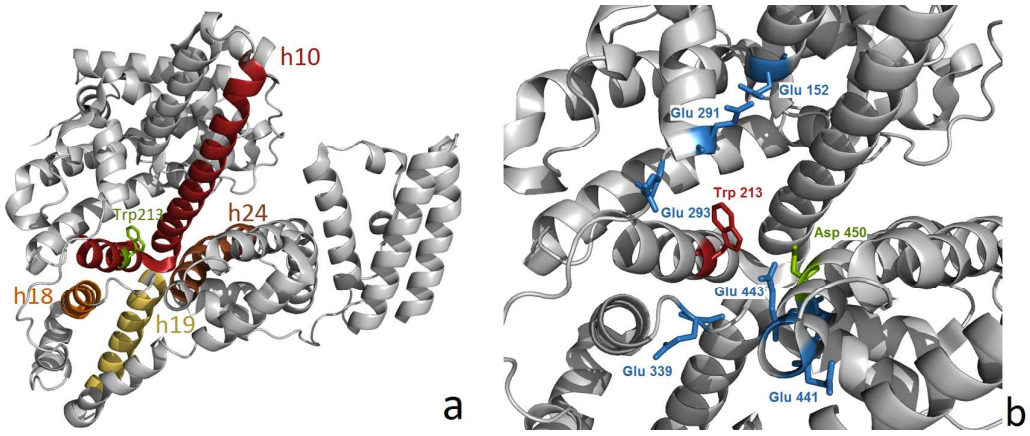

Figure 8. Trp213 is in a hydrophobic cavity surrounded by hydrophobic helices h10, h18, h19 and h24 (a). The cavity is also rich in Asp and Glu (b). The docking position of Pt-Blue is suggested to be the hydrophobic cavity around Trp213, possibly coordinated by residues Glu152, 291, 293, 339, 441, 443, 449 and Asp450.

The secondary structure analysis enabled us to identify individual bands representing secondary structure elements. Side chain contribution has been subtracted prior to curve-fitting in order to correlate the fitted bands to ordered structures. The band at 1685 cm^{-1} that showed up in previous analyses is absent in curve-fitting, which suggests that the origin of the band to be a side chain like Asn and Gln, but not hydrophobic loops/turns. In this respect, we suggest that Pt-Blue interacts with polar residues such as Gln220, Asn457 and Gln195 in the same hydrophobic cavity with Trp213. According to curve-fitting analysis, addition of Pt-Blue reduced the fraction of buried (hydrophobic) helices and increased the fraction of solvent exposed helices and/or unordered structure. The percentage fraction of this re-arrangement is estimated to be 15%, which approximately involves 90 a.a. in the process. We suggest that both partial unfolding and increased hydrophilicity around helices take place together during Pt-Blue docking. However, we also suggest that changes around helices outweigh the partial unfolding in this process in terms of the number of amino acids involved based on unpublished results of protein stability measurements. Thus, rather than major secondary structure changes, we conclude that re-arrangement of helices dominates the alterations reflected by the spectra. A good drug candidate should not change the structure of a carrier protein by more than ~10%, which would make the protein unrecognizable by its receptor [51]. Moreover, noncovalent interactions governing the association of Pt-Blue to BSA are another advantage since the drug is easily delivered to tumor cells and is available to bind to DNA. Therefore, the findings in this report lead to the conclusion that Pt-Blue is a promising anti-cancer drug candidate in terms of its kind and degree of interaction with BSA; however, further studies are needed before the clinical trials.

Supporting Information Available: UV-Vis absorption spectrum of blank BSA and blank Pt-Blue, curve-fitting of amide-I band of BSA with and without Pt-Blue and the second derivative of difference spectra given in Fig. 7a-inset are given.

ACKNOWLEDGMENT

This work is supported by the grants ATU-ALP-1011-01 and ATU-BAP/2006/04 provided by Atilim University. We thank Prof. Dr. Erik Goormaghtigh from Université Libre de Bruxelles, Belgium, for generously providing us with the software Kinetics for side chain subtraction. Authors also acknowledge Dr. Hakan Kayi for his valuable contributions during the preparation of the manuscript.

REFERENCES

1. J. P. Davidson, P. J. Faber, R. G. Fischer, S. Mansy, H. J. Peresie, B. Rosenberg, and L. VanCamp, *Cancer Chemother. Rep.*, 1975, **59**, 287–300.

2. A. H. Calvert, S. J. Harland, D. R. Newell, Z. H. Siddik, A. C. Jones, T. J. McElwain, S. Raju, E. Wiltshaw, I. E. Smith, J. M. Baker, M. J. Peckham, and K. R. Harrap, *Cancer Chemother. Pharmacol.*, 1982, **9**, 140–7.

3. S. G. Allan and J. F. Smyth, *Br. J. Cancer*, 1986, **53**, 355–60.

4. G. A. Curt, J. J. Grygiel, B. J. Corden, R. F. Ozols, R. B. Weiss, D. T. Tell, C. E. Myers, and J. M. Collins, *Cancer Res.*, 1983, **43**, 4470–3.

5. H. Akaza, M. Togashi, Y. Nishio, T. Miki, T. Kotake, Y. Matsumura, O. Yoshida, and Y. Aso, *Cancer Chemother. Pharmacol.*, 1992, **31**, 187–92.

6. G. Mathé, Y. Kidani, K. Triana, S. Brienza, P. Ribaud, E. Goldschmidt, E. Ecstein, R. Despax, M. Musset, and J. L. Misset, *Biomed. Pharmacother.*, 1986, **40**, 372–6.

7. E. P. Mitchell, *Oncology (Williston Park).*, 2000, **14**, 30–2.

8. S. L. Kelley and M. Rozencweig, *Eur. J. Cancer Clin. Oncol.*, 1989, **25**, 1135–40.

9. C. Tejel, M. A. Ciriano, and L. A. Oro, *Chem. - A Eur. J.*, 1999, **5**, 1131–1135.

10. K. Matsumoto and K. Sakai, *Adv. Inorg. Chem.*, 1999, **49**, 375–427.

11. K. A. Hofmann and G. Bugge, *Berichte der Dtsch. Chem. Gesellschaft*, 1908, **41**, 312–314.

12. R. D. Gillard and G. Wilkinson, *J. Chem. Soc.*, 1964, 1368.

13. C. M. A. Brett and A. M. O. Brett, *Electrochemistry: Principles, Methods and Applications*, Oxford University Press, USA, 1993.

14. A. Erdem and M. Ozsoz, *Electroanalysis*, 2002, **14**, 965–974.

15. T. Hirohama, Y. Kuranuki, E. Ebina, T. Sugizaki, H. Arii, M. Chikira, P. Tamil Selvi, and M. Palaniandavar, *J. Inorg. Biochem.*, 2005, **99**, 1205–19.

16. İ. Erilhan, Master of Science Thesis in Chemistry, Middle East Technical University, Ankara, Turkey, 2007.

17. J. J. Gullo, C. L. Litterst, P. J. Maguire, B. I. Sikic, D. F. Hoth, and P. V Woolley, *Cancer Chemother. Pharmacol.*, 1980, **5**, 21–6.

18. F. a de Wolf and G. M. Brett, *Pharmacol. Rev.*, 2000, **52**, 207–36.

19. K. A. Majorek, P. J. Porebski, A. Dayal, M. D. Zimmerman, K. Jablonska, A. J. Stewart, M. Chruszcz, and W. Minor, *Mol. Immunol.*, 2012, **52**, 174–82.

20. T. Peters, *All about albumin. Biochemistry, genetics and medical applications*, Academic Press, 1995.

21. E. Goormaghtigh, V. Cabiaux, and J. M. Ruysschaert, *Subcell. Biochem.*, 1994, **23**, 363–403.

22. J. F. Neault and H. A. Tajmir-Riahi, *Biochim. Biophys. Acta*, 1998, **1384**, 153–9.

23. F. Korkmaz, S. Köster, O. Yildiz, and W. Mäntele, *Spectrochim. Acta. A. Mol. Biomol. Spectrosc.*, 2012, **91**, 395–401.

24. A. Barth, *Biochim. Biophys. Acta*, 2007, **1767**, 1073–101.

25. J. K. Barton, D. J. Szalda, H. N. Rabinowitz, J. V. Waszczak, and S. J. Lippard, *J. Am. Chem. Soc.*, 1979, **101**, 1434–1441.

26. C. Vigano, M. Smeyers, V. Raussens, F. Scheirlinckx, J. M. Ruysschaert, and E. Goormaghtigh, *Biopolymers*, 2004, **74**, 19–26.

27. Venyaminov SYu and N. N. Kalnin, *Biopolymers*, 1990, **30**, 1243–1257.

28. X. Zhang, S. Li, L. Yang, and C. Fan, *Spectrochim. Acta. A. Mol. Biomol. Spectrosc.*, 2007, **68**, 763–70.

29. G. Mandal, M. Bardhan, and T. Ganguly, *Colloids Surf. B. Biointerfaces*, 2010, **81**, 178–84.

30. A. Buranaprapuk, C. V Kumar, S. Jockusch, and N. J. Turro, *Tetrahedron*, 2000, **56**, 7019–7025.

31. L. Xu, Y. Liu, W. Mei, X. Huang, and T. Chen, *Chem. Res. Chinese Univ.*, 2010, **26**, 693–698.

32. P. B. Kandagal, S. Ashoka, J. Seetharamappa, S. M. T. Shaikh, Y. Jadegoud, and O. B. Ijare, *J. Pharm. Biomed. Anal.*, 2006, **41**, 393–9.

33. P. Kalaivani, R. Prabhakaran, M. V. Kaveri, R. Huang, R. J. Staples, and K. Natarajan, *Inorganica Chim. Acta*, 2013, **405**, 415–426.

34. S. Nafisi, G. Bagheri Sadeghi, and A. PanahYab, *J. Photochem. Photobiol. B.*, 2011, **105**, 198–202.

35. K. R. Grigoryan and A. G. Kazaryan, *J. Appl. Spectrosc.*, 2009, **76**, 607–610.

36. T. Mukherjee, B. Sen, E. Zangrando, G. Hundal, B. Chattopadhyay, and P. Chattopadhyay, *Inorganica Chim. Acta*, 2013, **406**, 176–183.

37. R. R. G. Maciel, A. A. de Almeida, O. G. C. Godinho, F. D. S. Gorza, G. C. Pedro, T. F. Trescher, J. R. Silva, and N. C. de Souza, *Biomed Res. Int.*, 2013, **2013**, 1–7.

38. P. Daneshegar, A. A. Moosavi-Movahedi, P. Norouzi, M. R. Ganjali, M. Farhadi, and N. Sheibani, *J. Brazilian Chem. Soc.*, 2012, **23**, 315–321.

39. A. Bujacz, *Acta Crystallogr. D. Biol. Crystallogr.*, 2012, **68**, 1278–89.

40. A. Barth, *Prog. Biophys. Mol. Biol.*, 2000, **74**, 141–173.

41. H. Fabian and W. Maentele, in *Handbook of Vibrational Spectroscopy*, eds. J. M. Chalmers and P. R. Griffiths, John Wiley and Sons, Chichester, 2006, pp. 3399–3426.

42. S. Sukumaran, K. Hauser, E. Maier, R. Benz, and W. Mäntele, *Biochemistry*, 2006, **45**, 3972–80.

43. J. L. Arrondo, a Muga, J. Castresana, and F. M. Goñi, *Prog. Biophys. Mol. Biol.*, 1993, **59**, 23–56.

44. L. K. Tamm and S. a Tatulian, *Q. Rev. Biophys.*, 1997, **30**, 365–429.

45. S. Mukherjee, P. Chowdhury, and F. Gai, *J. Phys. Chem. B*, 2007, **111**, 4596–602.

46. J. Grdadolnik and Y. Maréchal, *Biopolymers*, 2001, **62**, 40–53.

47. P. I. Haris and D. Chapman, *Biopolymers*, 1995, **37**, 251–63.

48. E. Goormaghtigh, J.-M. Ruysschaert, and V. Raussens, *Biophys. J.*, 2006, **90**, 2946–57.

49. E. Goormaghtigh, *Eur. J. Biochem.*, 2005, **193**, 409–420.

50. Y. Wang, X. Wang, J. Wang, Y. Zhao, W. He, and Z. Guo, *Inorg. Chem.*, 2011, **50**, 12661–8.

51. A. R. Timerbaev, C. G. Hartinger, S. S. Aleksenko, and B. K. Keppler, *Chem. Rev.*, 2006, **106**, 2224–48.